

Level-to-level and total probability for Auger decay including direct double processes of Ar $2p^{-1}$ hole states

Jiaolong Zeng,^{*} Pengfei Liu, Wenjun Xiang, and Jianmin Yuan

Department of Physics, College of Science, National University of Defense Technology, Changsha Hunan, People's Republic of China, 410073

(Received 4 March 2013; published 26 March 2013)

Auger decay including direct double processes of Ar $2p^{-1}$ hole levels is investigated in the framework of perturbation theory implemented by distorted wave approximation with balanced large-scale configuration interaction among the successive ions being taken into account. The complex transition amplitude obtained from the second perturbation theory for the direct double Auger decay (DAD) is decomposed into approximate formulas according to two generally agreed mechanisms of shake-off and knock-out. Practical computations showed that the knock-out condition is fulfilled and thus justified such a decomposition treatment of knock-out mechanism. The contribution to the DAD probability from knock-out mechanism is larger than shake-off by an order of magnitude and therefore the former is dominant. The interference effect between the knock-out and shake-off mechanisms should be trivial and neglecting it we obtained a branching ratio of 12.0% for the direct DAD into triply charged states of Ar³⁺. By including cascade double decay, a total branching ratio of 14.9% is obtained. Our result explained recent experimental results on the branching ratio into triply charged ion, and should be useful for further detailed experimental investigations.

DOI: [10.1103/PhysRevA.87.033419](https://doi.org/10.1103/PhysRevA.87.033419)

PACS number(s): 32.80.Hd, 31.15.am, 32.80.Zb

I. INTRODUCTION

Absorption of (soft) x-ray photon by atoms or molecules leads to the formation of charged ion with the production of inner-shell vacancies. The advent of extreme ultraviolet (EUV) [1,2] and x-ray [3,4] free-electron lasers made such core hole states a common phenomenon in the interaction of ultraintense, short-pulsed (soft) x rays with atoms and molecules [5–11]. To model the x-ray interaction with matter, one needs a large number of atomic data including cascade and direct multiple Auger decay rates [12]. The direct double Auger decay (DAD) is one of the most important second-order processes, where two electrons are ejected simultaneously from an inner-shell excited atom upon radiationless decays. For the Auger decay including direct DAD process, extensive experimental studies were carried out during the past several decades, however, quantitative theoretical explanation is lacking very much.

The first experimental evidence of direct DAD processes was discovered in the experiments on detection of photoions formed from *K*-shell photoionization of neon by using x rays with energy between 867 and 913 eV [13,14]. Studies of the Auger electron spectra in Ar followed [15], where a measured Auger electron continuum was suggested to originate from a double decay process. Since then, more accurate experiments were carried out by using synchrotron radiation or x-ray lasers and coincidence techniques for the inner-shell vacancies of argon [16–20]. Alkemper, Doppelfeld, and Busch [16] experimentally investigated $L_{2,3}MMM$ Auger spectrum of *K*-ionized argon by using a decomposition of electron-ion and electron-electron coincidence techniques. The decay of Ar $2p^{-1}$ and $2s^{-1}$ hole states was investigated by means of photoelectron-ion coincidence spectroscopy [17]. Double decay fraction into third ionized states of Ar³⁺ contributes considerably to the decay process of the Ar $2p^{-1}$ (13%)

hole state, and the dominant contribution is due to the direct DAD process. Further work showed an enhancement of DAD probability in xenon clusters irradiated with a soft-x-ray laser pulse with a wavelength of 13.9 nm and an intensity of up to 2×10^{10} W/cm² using a time-of-flight ion mass spectrometer [18]. Possible mechanisms responsible for the enhancement of rates are discussed, yet quantitative theoretical explanation is lacking. Viefhaus *et al.* [19] observed the direct $L_{2,3}MMM$ decay after photoionization of the $2p$ shell of argon by angle-resolved electron-electron coincidence spectroscopy. The measured energy and angular distributions of the emitted electrons can gain a further insight into this three-body Coulomb process. Recently, a study was carried out for the Auger decay including DAD process of argon $2p$ satellite states by using a multielectron coincidence technique [20]. Complex decay patterns involving both radiative and nonradiative decays following core $1s$ photoionization of Ar were investigated by measuring the recoil energy of the ions during the emission of Auger electrons [21]. Multiple Auger decays can be used to investigate the ultrafast dynamics in inner-shell photoionization [22], but complete understanding of the dynamics needs detailed theoretical information on the Auger decay rates including direct double process.

From the above description, one knows that significant experimental advancements were made during the past decades, yet theoretical interpretation is lacking very much for the direct DAD process. There has not been theoretical explanation for the experimental work mentioned above [16–20], even qualitatively. Yet, some theoretical research has been devoted to the direct double decay process. To the best of our knowledge, there is only one theoretical prediction on the DAD probability of Ar $2p^{-1}$ by employing a shake-off mechanism [23], which strongly underestimated the decay fraction into higher charged ions of Ar³⁺. Theoretical investigations of the DAD process of Ar $2p^{-1}$ by using a knock-out mechanism have also been lacking. Thus the experimental measured branching ratio for the decay into triply charged states [17,19,20] has not been

^{*}jlzeng@nudt.edu.cn

explained theoretically. Therefore, there is a strong necessity to carry out such theoretical studies to fully understand the experimental results.

In this work, we investigate the Auger decay including the direct DAD process for Ar $2p^{-1}$ by using a distorted wave approximation which takes into account large-scale configuration interaction (CI). Both shake-off and knock-out mechanisms are considered in the calculations. The detailed level-to-level rates and the relative fraction of double to total Auger process were obtained with balanced electron correlations for the successive ions. The Auger decay process is entirely due to the interaction of electrons, and thus a balanced treatment of electron correlations is important for obtaining accurate results. Comparison is made with available experimental results and good agreement was found for the branching ratio of DAD probability to the total Auger decay rate.

II. THEORETICAL METHOD

A relativistic approach based on the Dirac equation is used throughout the entire calculations. The atomic structure is determined by diagonalizing the relativistic Hamiltonian (atomic unit is used in this section) [24]:

$$H = \sum_{i=1}^N H_D(i) + \sum_{i<j}^N \frac{1}{r_{ij}}, \quad (1)$$

where $H_D(i)$ is the single-electron Dirac Hamiltonian for the potential due to the nuclear charge and N is the number of bound electrons. The basis states ϕ_j , which are referred to as configuration state functions (CSFs), are antisymmetric sums of the products of N one-electron Dirac spinors $\varphi_{n\kappa m}$,

$$\varphi_{n\kappa m} = \frac{1}{r} \begin{pmatrix} P_{n\kappa}(r)\chi_{\kappa m}(\theta, \psi, \sigma) \\ iQ_{n\kappa}(r)\chi_{-\kappa m}(\theta, \psi, \sigma) \end{pmatrix}, \quad (2)$$

where $P_{n\kappa}(r)$ and $Q_{n\kappa}(r)$ are radial functions for the large and small components of the orbital, and where $\chi_{\kappa m}(\theta, \psi, \sigma)$ is a two-component spherical spinor; n , κ , and m are the principal, relativistic angular, and magnetic quantum number, respectively. The relativistic angular quantum number κ is linked with nonrelativistic (l) and total (j) angular quantum number by $\kappa = (l - j)(2j + 1)$. The large and small components, $P_{n\kappa}(r)$ and $Q_{n\kappa}(r)$, satisfy the coupled Dirac equation for a local central field in the standard Dirac-Fock-Slater method. The local central potential includes the contributions from the nuclear charge and the electron-electron interaction [24]. The standard jj coupling scheme is used in coupling the angular momenta of successive shells. Various orbitals are assumed to be orthonormal:

$$\int_0^\infty (P_{n\kappa} P_{n'\kappa} + Q_{n\kappa} Q_{n'\kappa}) dr = \delta_{nn'}. \quad (3)$$

An atomic state is approximated by a linear combination of CSFs with the same symmetry:

$$\Psi_i(J\pi) = \sum_j^{n_c} a_j \phi_j(J\pi), \quad (4)$$

where n_c is the number of CSFs and a_j denotes the representation of the atomic state in this basis.

In the first-order perturbation theory, single Auger decay rate can be written as [25]

$$A_{\text{im}}^1 = \frac{4}{k_m} |\langle \Psi_m^+ | V | \Psi_i \rangle|^2, \quad (5)$$

where k_m is the momentum of the Auger electron, the perturbation V is the Coulomb operator of two-electron interaction potential, $|\Psi_i\rangle$ is the initial autoionizing level of an ion with charge q , and $|\Psi_m^+\rangle$ is the intermediate level of an ion with charge $q + 1$ plus a continuum electron:

$$|\Psi_m^+\rangle = \sum_{\kappa} |\Psi_m, \kappa; J_T M_T\rangle, \quad (6)$$

where the intermediate state $|\Psi_m\rangle$ has one less electron than $|\Psi_i\rangle$, J_T is the total angular momentum when the target state is coupled to the continuum orbital, M_T is the projection of the total angular momentum, and κ is the relativistic angular quantum number of the free electron, whose wave functions are obtained by solving the Dirac equations with the same central potential as that for bound orbitals of $|\Psi_m\rangle$. For the continuum, the radial grid is divided into two regions. In the inner region, where the wave function is not oscillatory, or the oscillation period is large enough to contain a sufficient number of grid intervals, the standard Numerov method is used to integrate the equation outward. Beyond some point $r = r_c$, which depends on the energy and angular momentum of the continuum sought, the oscillation period of the wave function becomes too small for the direct integration to be accurate. At that point, a phase-amplitude method is employed. The inner and outer solutions are matched at r_c by requiring the continuity of the radial wave function and its first derivative. The detailed implementation of the formalism can be found in Ref. [24].

The wave functions $|\Psi_i\rangle$ and $|\Psi_m\rangle$ of the initial and intermediate levels are represented by a CI-type expansion like Eq. (4) and the wave function of continuum electron is normalized according to the standard procedure of continuum states. The total energy $E = \varepsilon_i$ for the initial level and $E = \varepsilon_m^+ + k_m^2/2$ for the intermediate level with k_m being the momentum of the Auger electron.

Direct DAD rate in the lowest-order perturbation theory is given by

$$A_{\text{if}}^2 = \frac{8}{\pi} \int_0^{k_{\text{max}}} \frac{dk_{f1}}{k_{f2}} \left| \sum_m \sum_{k_m} \frac{\langle \Psi_f^{2+} | V | \Psi_m^+ \rangle \langle \Psi_m^+ | V | \Psi_i \rangle}{\varepsilon_i - \varepsilon_m^+ - k_m^2/2} \right|^2, \quad (7)$$

where $|\Psi_f^{2+}\rangle$ is the final level of an ion with charge $q + 2$ plus two continuum electrons, which is similarly constructed as in Eq. (6). The total energy $E = \varepsilon_f^{2+} + E_{\text{max}}$ should be conserved with that of the initial level $E = \varepsilon_i$, where $E_{\text{max}} = k_{f1}^2/2 + k_{f2}^2/2$ with k_{f1} and k_{f2} being the momenta of the two Auger electrons, respectively. The energy for the (quasi-)bound levels of ε_i , ε_m , and ε_f is relative to that of the ground level of the initial ion. The energy conservation relation means that the total energy of the two Auger electrons is fixed yet the energy of any one electron can be varied from zero to the maximum E_{max} . Thus we set $k_{\text{max}} = \sqrt{E_{\text{max}}}$, which corresponds to an upper limit in an integration over the energy

of $E_{\max}/2$ to avoid a double counting of the continuum states. The summations over intermediate middle level $|\Psi_m^+\rangle$ in the expression of A_{if}^2 for the direct double Auger rate include a summation over all possible $(q+1)$ ion levels and a summation over a complete set of bound and continuum states of the remaining electron. The intermediate middle level summations are calculated by summing over a finite number of bound levels and then integrating over continuum states. The vanishing denominator $D = \varepsilon_i - \varepsilon_m^+ - k_m^2/2$ are replaced by

$$\lim_{\eta \rightarrow 0} (D + i\eta)^{-1} = P D^{-1} - i\pi \delta(D), \quad (8)$$

where P denotes a principal-value integration. From the above definition of single and direct double decay rates, one can see that these two processes are entirely due to the interaction between electrons of autoionized ion, and therefore a proper treatment of the wave functions of $|\Psi_i\rangle$, $|\Psi_m^+\rangle$, and $|\Psi_f^{2+}\rangle$ is vital to obtain accurate results.

From Eq. (7), one can see that the most important quantity in the calculation of the DAD rates is the computation of the transition amplitude, which is so complex that one must include a summation over many multielectron continua as well as the integration over the single-electron continuum of the emitted electron and a principal-value integration. To simplify the computation, we present approximate formulas according to two generally agreed mechanisms: shake-off (SO) and knock-out (KO) [26]. In the SO process, the primary electron is ejected rapidly after Auger decay and a subsequent transition of the remaining electron to the continuum takes place due to a sudden change of the atomic potential. The sudden approximation properly describes the double decay process in the high-energy limit for the Auger electron. At a lower Auger electron energy, the KO mechanism should dominate for a relatively shallow vacancy such as Ar $2p^{-1}$.

In the KO mechanism, the imaginary part is much larger than the real part in Eq. (8) and therefore the former dominates in the total transition amplitude. By simple analysis neglecting the contribution from the real part, the direct DAD rate for an initial state $|\Psi_i\rangle$ to a final one $|\Psi_f^{2+}\rangle$ can be written as

$$A_{\text{KO}}^2 = \sum_m A_{\text{im}}^1 \sigma_{\text{mf}}(\varepsilon_0), \quad (9)$$

where A_{im}^1 is the single Auger decay rate from the initial hole level i to a middle level m and $\sigma_{\text{mf}}(\varepsilon_0)$ is the cross section of the inelastic scattering of the ‘‘intermediate’’ Auger electron upon the middle level m to the final level f , where the energy of free electron ε_0 satisfies the energy conservation law.

In the SO mechanism, the direct DAD rates can be decomposed into the following formula [26]:

$$A_{\text{SO}}^2 = \sum_m A_{\text{im}}^1 |\langle \Psi_f^{2+} | \Psi_m^+ \rangle|^2, \quad (10)$$

where the matrix element $\langle \Psi_f^{2+} | \Psi_m^+ \rangle$ means the overlap integral between the two wave functions determined in the field of the initial level i and in the field of vacancies with two Auger electrons being emitted.

In general, there is an interference effect between different mechanisms and therefore one should add the KO and SO transition amplitudes rather than the DAD rates. For double photoionization, researches showed that two

contributing mechanisms (SO and KO) can be separated due to a quasiclassical nature of KO and a purely quantum characteristic of SO [27,28]. The DAD process is similar to double photoionization in the physical mechanism; both emit two electrons simultaneously. Therefore, we suggest that such a separation of mechanisms should apply to the direct DAD process as well. In this work, we investigate the DAD rates according to such a procedure.

III. RESULTS AND DISCUSSION

From the approximate formulas (9) and (10), we know that the single Auger process is the first step of both KO and SO mechanisms, therefore the accurate SAD rate is pivotal to calculate the DAD rates. A single Auger process has been well investigated by using various theoretical methods [29], and it is not our focus in this work. Single and double Auger decay processes are strictly due to electron-electron interaction and hence CI effect plays an important role in accurately determining the rates [30–33]. In this work, large-scale CI calculations were carried out to obtain the single and double Auger decay rates for the hole levels belonging to configuration $1s^2 2s^2 2p^5 3s^2 3p^6$ of Ar⁺. The DAD process concerns bound state wave functions of three different successive ionization stages, i.e., Ar⁺, Ar²⁺, and Ar³⁺; a balanced treatment of electron correlations for these ions is vital to properly describe such a process. Single and double excitations from the respective ground configurations of Ar⁺, Ar²⁺, and Ar³⁺ to orbitals of $3d$, $4s$, $4p$, and $4d$ are considered for the electron correlations. Taking Ar⁺ as an example to illustrate the scale of CI, the interactions among the fine-structure levels belonging to the following configurations are included: $[1s^2 2s^2 2p^6] 3s^2 3p^5$, $3s^2 3p^4 nl$, $3s 3p^6$, $3s 3p^5 nl$, $3s^2 3p^3 nl n'l'$, $3s 3p^4 nl n'l'$, $3p^5 nl n'l'$, $[1s^2 2s^2] 2p^5 3s^2 3p^6$, $2p^5 3s^2 3p^5 nl$, $2p^5 3s 3p^6 nl$, $2p^5 3s^2 3p^4 nl n'l'$, and $2p^5 3s 3p^5 nl n'l'$ ($nl, n'l' = 3d, 4s, 4p$, and $4d$).

There are so many autoionizing channels for the decay of Ar $2p^{-1}$ that it is not necessary to present all of them here. As illustrative examples, Table I lists fine-structure level-to-level SAD rates for the dominant channels with a value larger than $5.0 \times 10^{12} \text{ s}^{-1}$. It can be seen that the most important channels are due to levels of $3s^2 3p^4$ configuration, which account for 75% of the total rate. The next strongest channels originate from levels of the $3s 3p^5$ configuration with a contribution of 12%. Such a conclusion was also observed in earlier work [34–36]. Except for these strong channels, there are some weak ones originating from configurations such as $3p^6$, $3s^2 3p^2 3d^2$, $3s 3p^4 3d$, and $3p^5 3d$. The energy of levels belonging to these configurations are higher than the ionization potential of Ar²⁺ (with ground configuration $3s^2 3p^4$), and as a result, they will decay to Ar³⁺ via the cascade double Auger process. The strongest channel for these cascade double decay processes is due to $3p^6$ with a rate of $1.753 \times 10^{12} \text{ s}^{-1}$. The total rate for these cascade channels is 6.09×10^{12} and $6.12 \times 10^{12} \text{ s}^{-1}$, respectively, for levels of Ar $2p_{3/2}^{-1}$ and $2p_{1/2}^{-1}$.

As a comparison, the transition energy and SAD rate obtained by Bruneau [34], who employed a multiconfiguration Dirac-Fock program by using Slater’s transition state approximation, are also given in the last two columns in Table I. Although the trends in both calculations are similar,

TABLE I. Fine-structure level-to-level single Auger decay probability A^1 (s^{-1}) for the main channels of Ar $2p^{-1}$ hole states with a value larger than $5.0 \times 10^{12} s^{-1}$. Figures in brackets indicate powers of ten. The first three columns refer to the initial $2p^{-1}$ level, final state designation, and angular momentum J , respectively, and the last four columns to transition energy ΔE (in eV) and Auger decay rates obtained in this work and by Bruneau.

Level	Final state	J	ΔE	A^1	ΔE [34]	A^1 [34]
$2p_{3/2}^{-1}$	$3s^2 3p_{1/2}^2 3p_{3/2}^2$	2	206.37	4.79(13)	206.82	6.15(13)
$2p_{3/2}^{-1}$	$3s^2 3p_{1/2} 3p_{3/2}^3$	1	206.26	1.70(13)	206.66	2.15(13)
$2p_{3/2}^{-1}$	$3s^2 3p_{1/2} 3p_{3/2}^3$	2	204.41	5.70(13)	204.71	6.89(13)
$2p_{3/2}^{-1}$	$3s^2 3p_{1/2}^2 3p_{3/2}^2$	0	202.07	1.32(13)	202.09	1.43(13)
$2p_{3/2}^{-1}$	$3s_{1/2} 3p_{1/2}^2 3p_{3/2}^3$	2	190.59	1.20(13)	189.60	2.30(13)
$2p_{3/2}^{-1}$	$3s_{1/2} 3p_{1/2}^2 3p_{3/2}^3$	1	187.01	6.64(12)		
$2p_{3/2}^{-1}$	$3s^2(3p_{1/2}(3p_{3/2}^2)_2)_{5/2} 4p_{3/2}$	1	177.62	9.36(12)		
$2p_{3/2}^{-1}$	All channels			1.845(14)		2.66(14)
$2p_{1/2}^{-1}$	$3s^2 3p_{1/2}^2 3p_{3/2}^2$	2	208.50	1.62(13)	209.08	2.30(13)
$2p_{1/2}^{-1}$	$3s^2 3p_{1/2} 3p_{3/2}^3$	1	208.39	3.35(13)	208.92	4.95(13)
$2p_{1/2}^{-1}$	$3s^2 3p_{3/2}^4$	0	208.29	1.37(13)	208.85	1.99(13)
$2p_{1/2}^{-1}$	$3s^2 3p_{1/2} 3p_{3/2}^3$	2	206.54	6.01(13)	206.97	8.57(13)
$2p_{1/2}^{-1}$	$3s^2 3p_{1/2}^2 3p_{3/2}^2$	0	204.20	1.56(13)	205.16	2.09(13)
$2p_{1/2}^{-1}$	$3s^2 3p_{1/2} 3p_{3/2}^4$	1	192.64	8.96(12)	191.70	2.03(13)
$2p_{1/2}^{-1}$	$3s 3p_{1/2}^2 3p_{3/2}^3$	1	189.14	7.38(12)		
$2p_{1/2}^{-1}$	$3s^2(3p_{1/2}(3p_{3/2}^2)_2)_{5/2} 4p_{3/2}$	1	179.75	9.84(12)		
$2p_{1/2}^{-1}$	All channels			1.840(14)		2.31(14)

obvious discrepancy was found between the two results, which should be a result of different treatment of the CI. From the comparison, one can find that the transition energy predicted by Bruneau [34] is just a little higher than our results for higher Auger transition energy and a little lower for lower Auger transition energy, yet the rates are systematically larger than our calculated values. Bruneau [34] predicted a total decay rate of 2.66×10^{14} and $2.31 \times 10^{14} s^{-1}$, respectively, for levels of Ar $2p_{3/2}^{-1}$ and $2p_{1/2}^{-1}$, which are also larger than our values of 1.845×10^{14} and $1.840 \times 10^{14} s^{-1}$. In our investigation, a larger scale of CI was used and our results should be more converged, which can be more clearly seen by comparing the theoretical lifetimes with the experiments. The natural lifetime width is directly connected with the total decay rate,

$$\Gamma = \hbar \sum_{j < i} A_{ij}^1. \quad (11)$$

Our calculated lifetime widths are compared with experimental values [37–42] in Table II. From the inspection of Table II, the experimental Auger widths [37–42] range from 100 to 130 meV with errors being less than or equal to 10 meV for both levels of $2p_{3/2}^{-1}$ and $2p_{1/2}^{-1}$. Our theoretical natural width of 121 meV is within the error bars of the experiments [37–41],

yet the results obtained by Bruneau [34] (174 and 151 meV for $2p_{3/2}^{-1}$ and $2p_{1/2}^{-1}$, respectively) are larger than experimental values and outside the error bars of all these observed Auger widths [37–42].

After checking the validity of the treatment of the SAD process, we now turn on the direct DAD rates for Ar $2p^{-1}$, which are shown in Table III for the dominant channels in fine-structure levels with a rate larger than $5.0 \times 10^{11} s^{-1}$. The contributions of the real and imaginary parts of the transition amplitude to the KO DAD rates are given in the fifth and sixth columns, while that of the SO mechanism is listed in the last column of Table III. Meaningful conclusions can be drawn for the direct double decay process of Ar $2p^{-1}$ hole levels from the inspection of Table III. First, we point out that the condition of KO mechanism is indeed fulfilled. The contribution from the real matrix elements to the DAD rates is more than two orders of magnitude smaller than that of the imaginary part for the KO mechanism, verifying that the imaginary part does dominate in the KO total transition amplitude, which is the condition that KO holds as discussed in the above. Such a fact means that the direct DAD rates contributed by KO mechanism obtained from Eq. (9) is valid for the practical computations. Second, the interference effect between the KO and SO mechanisms is small compared with the contribution of KO mechanism. In

TABLE II. Lifetime widths (meV) of the Ar $2p^{-1}$ hole states compared with the experimental values from the literature, with the errors given in parentheses. Numbers in square brackets refer to sources of literatures from which values are taken.

Level	This work	Bruneau [34]	Expt.
$2p_{3/2}^{-1}$	121	174	118(4) [37], 120 [40], 130(5) [41], 130 [39], 100(10) [42]
$2p_{1/2}^{-1}$	121	151	118(4) [37], 120 [40], 130(5) [41], 130 [39], 107(10) [42], 120 [38]

TABLE III. Level-to-level direct DAD rates (s^{-1}) for the dominant channels of Ar $2p^{-1}$ hole levels. The transition energy ΔE , the contributions of the imaginary (I A_{KO}^2) and real (R A_{KO}^2) parts of the transition amplitude to the KO DAD rates, and the contribution from the SO mechanism are given in the last four columns. Figures in brackets indicate powers of ten.

Level	Final level	J	ΔE	I A_{KO}^2	R A_{KO}^2	A_{SO}^2
$2p_{3/2}^{-1}$	$3s^2 3p_{1/2}(3p_{3/2}^2)_2$	3/2	168.02	2.258(12)	7.084(9)	2.090(11)
$2p_{3/2}^{-1}$	$3s^2 3p_{1/2}(3p_{3/2}^2)_2$	5/2	164.66	6.013(12)	1.534(10)	4.463(11)
$2p_{3/2}^{-1}$	$3s^2 3p_{1/2}(3p_{3/2}^2)_1$	3/2	164.65	3.072(12)	9.165(9)	2.538(11)
$2p_{3/2}^{-1}$	$3s^2 3p_{1/2}(3p_{3/2}^2)_0$	1/2	163.71	1.626(12)	5.220(9)	9.087(10)
$2p_{3/2}^{-1}$	$3s^2 3p_{3/2}^3$	3/2	163.70	2.801(12)	9.286(9)	2.796(10)
$2p_{3/2}^{-1}$	$3s_{1/2} 3p_{1/2}^2(3p_{3/2}^2)_2$	5/2	154.99	1.147(12)	3.973(9)	2.941(9)
$2p_{3/2}^{-1}$	$(3s_{1/2} 3p_{1/2})_0 3p_{3/2}^3$	3/2	154.90	5.039(11)	2.013(9)	1.666(11)
$2p_{3/2}^{-1}$	$(3s_{1/2} 3p_{1/2})_1 3p_{3/2}^3$	3/2	152.47	7.512(11)	2.256(9)	1.192(11)
$2p_{3/2}^{-1}$	$(3s_{1/2} 3p_{1/2})_1 3p_{3/2}^3$	5/2	152.45	1.345(12)	4.239(9)	1.511(10)
$2p_{3/2}^{-1}$	$3s^2(3p_{1/2} 3p_{3/2})_2 3d_{5/2}$	3/2	145.35	4.018(11)	1.074(9)	7.869(9)
$2p_{1/2}^{-1}$	$3s^2 3p_{1/2}(3p_{3/2}^2)_2$	3/2	170.15	2.026(12)	6.830(9)	1.864(11)
$2p_{1/2}^{-1}$	$3s^2 3p_{1/2}(3p_{3/2}^2)_2$	5/2	166.79	5.278(12)	1.247(10)	4.246(11)
$2p_{1/2}^{-1}$	$3s^2 3p_{1/2}(3p_{3/2}^2)_1$	3/2	166.78	3.683(12)	1.116(10)	2.040(11)
$2p_{1/2}^{-1}$	$3s^2 3p_{1/2}(3p_{3/2}^2)_0$	1/2	165.84	1.715(12)	6.165(9)	6.292(10)
$2p_{1/2}^{-1}$	$3s^2 3p_{3/2}^3$	3/2	165.83	2.937(12)	9.309(9)	3.828(10)
$2p_{1/2}^{-1}$	$3s_{1/2} 3p_{1/2}^2(3p_{3/2}^2)_2$	5/2	157.12	4.292(11)	1.410(9)	5.384(8)
$2p_{1/2}^{-1}$	$(3s_{1/2} 3p_{1/2})_0 3p_{3/2}^3$	3/2	157.03	7.765(11)	3.020(9)	1.615(11)
$2p_{1/2}^{-1}$	$3s_{1/2} 3p_{3/2}^3$	1/2	158.24	5.174(11)	1.676(9)	1.338(9)
$2p_{1/2}^{-1}$	$(3s_{1/2} 3p_{1/2})_1 3p_{3/2}^3$	3/2	154.60	1.031(12)	3.089(9)	9.463(10)
$2p_{1/2}^{-1}$	$(3s_{1/2} 3p_{1/2})_1 3p_{3/2}^3$	5/2	154.58	1.119(12)	3.329(9)	1.658(10)

KO mechanism, there are seven strong double decay channels with a rate larger than $1.0 \times 10^{12} s^{-1}$ for both $2p_{3/2}^{-1}$ and $2p_{1/2}^{-1}$ levels, which can be seen from Table III. For every channel, the contribution of the SO mechanism (column 7 in Table III) is smaller than that of KO by more than an order of magnitude. Such a large difference means that the interference effect is trivial between the two mechanisms. Even assuming a maximal degree of interference between SO and KO transition amplitudes, its effect is less than 7% of the total DAD rates for the strong channels. Note that the interference effect can only occur between the transition amplitudes originating from the same channel of SO and KO mechanisms, which means there is no such effect from different channels. As a result, there is no interference effect from different rows in Table III. Therefore, we may safely estimate that this effect should be $<3\%$, which is smaller than or comparable with the best up-to-date experimental error bars, as will be discussed in the following. From these analyses, we know that the KO is the dominant mechanism in the direct DAD process of Ar $2p^{-1}$. In fact, such a conclusion is understandable as the SO mechanism is most applicable at the high-energy limit for the Auger electron. For Ar $2p^{-1}$ decay, the energy of the Auger electron is less than 200 eV, which is far below the high-energy limit, and therefore the SO mechanism is naturally not a good approximation.

To have a more complete physical picture of Ar $2p^{-1}$ Auger decay, we show the single (including cascade double) and direct double Auger spectra in Fig. 1. For one particular channel, its contribution to the spectra are obtained by including the lifetime broadening and an assumed instrument

resolution of 0.5 eV by using a Voigt profile,

$$I(E) = A \frac{\sqrt{\ln 2}}{\sqrt{\pi} \Gamma_g} H(a, v), \quad (12)$$

where $I(E)$ is the intensity of single or double Auger electrons at energy E which is the energy of Auger electron for SAD and the sum of two Auger electrons for direct DAD, A refers to the SAD A^1 or DAD A^2 rates which are obtained according to the above method, and $H(a, v)$ is the Voigt function [43]:

$$H(a, v) = \frac{a}{\pi} \int_{-\infty}^{+\infty} \frac{e^{-x^2}}{a^2 + (v-x)^2} dx,$$

$$a = \sqrt{\ln 2} \Gamma_l / \Gamma_g, \quad v = \sqrt{\ln 2} (E - \Delta E) / \Gamma_g,$$

where ΔE is the energy difference between the initial and final levels, and Γ_g and Γ_l are the Gaussian (instrumental) and Lorentzian (lifetime) half width at half maximum, respectively. The whole spectra are obtained by summing contributions over all possible channels. From the inspection of Fig. 1, one can see that the energy of some channels are so close that they coalesce together both for the single and double decay process. Besides for the strong channels given in Tables I and III, there are some weak channels as well, which originate from configurations such as $3p^6$ for SAD and $3p^5$ for the DAD process. Our theoretical spectra are in agreement with the experimental intensity taken at a photon energy of 270 eV (Fig. 3 in Vieffhaus *et al.* [19]) and at 251.63 eV (Fig. 1 in Sheinerman *et al.* [44]) after photoionization of the Ar $2p$

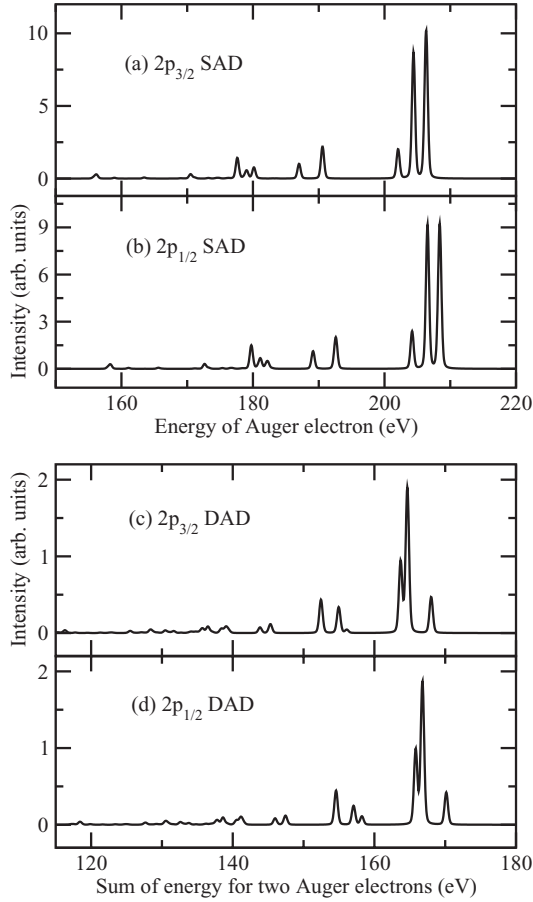


FIG. 1. Auger spectra for the single Auger decay of Ar (a) $2p_{3/2}^{-1}$, (b) $2p_{1/2}^{-1}$, and direct double Auger decay of (c) $2p_{3/2}^{-1}$, and (d) $2p_{1/2}^{-1}$.

shell except that the experimental resolution is lower so that the structures shown in Fig. 1 are merged together at an electron energy centered at ~ 163 eV [19], which is very close to our theoretical value ~ 165 eV in Fig. 1. The small difference between ~ 163 and ~ 165 eV might be due to the postcollision interactions occurring in the decay of Ar $2p^{-1}$ holes by emission of two Auger electrons [44].

To have a more direct and compact understanding of the direct DAD channels of Ar $2p^{-1}$, we transformed the level-to-level to level-to-configuration rates by summing all possible final levels belonging to one particular configuration, which is shown in Table IV. Two sets of theoretical results are given for the DAD rates and branching ratio to the dominant triply charged ion: one solely due to KO mechanism and another with both KO and SO contributing, which is denoted by symbols a and b , respectively. It can be seen from Table IV that the decay trends are basically the same for both sets of theoretical results. The most important contribution is due to configuration $3s^23p^3$ of Ar $^{3+}$, which accounts for 66.7% of the total rate and the next strongest configuration of $3s3p^4$ contributes a fraction of 18.2%. The other four configurations $3p^5$, $3s^23p^23d$, $3s^23p^24p$, and $3s3p^33d$ contribute 1.9%, 6.6%, 2.7%, and 1.8%, respectively. The total direct DAD rates for levels of $2p_{3/2}^{-1}$ and $2p_{1/2}^{-1}$ are 2.377×10^{13} and 2.374×10^{13} s $^{-1}$, respectively, for the KO mechanism and 2.520×10^{13} and 2.504×10^{13} s $^{-1}$ by including contributions

TABLE IV. Direct DAD rates (s $^{-1}$) and branching ratios (BR) η (%) of Ar $2p^{-1}$ to the dominant configurations of Ar $^{3+}$. Figures in brackets indicate powers of ten. The notations a and b represent results solely due to KO and both KO and SO mechanisms.

Level	Final config.	DAD rate ^a	BR η^a	DAD rate ^b	BR η^b
$2p_{3/2}^{-1}$	$3s^23p^3$	1.577(13)	66.3%	1.680(13)	66.7%
	$3s3p^4$	4.348(12)	18.3%	4.579(12)	18.2%
	$3p^5$	4.724(11)	2.0%	4.729(11)	1.9%
	$3s^23p^23d$	1.580(12)	6.6%	1.668(12)	6.6%
	$3s^23p^24s$	2.652(11)	1.1%	2.670(11)	1.1%
	$3s^23p^24p$	6.730(11)	2.8%	6.740(11)	2.7%
	$3s3p^33d$	4.548(11)	1.9%	4.618(11)	1.8%
	total	2.377(13)	100%	2.520(13)	100%
$2p_{1/2}^{-1}$	$3s^23p^3$	1.564(13)	65.9%	1.655(13)	66.1%
	$3s3p^4$	4.372(12)	18.4%	4.662(12)	18.6%
	$3p^5$	4.871(11)	2.1%	4.916(11)	1.9%
	$3s^23p^23d$	1.690(12)	7.1%	1.779(12)	7.1%
	$3s^23p^24s$	2.196(11)	0.9%	2.304(11)	0.9%
	$3s^23p^24p$	6.134(11)	2.6%	6.242(11)	2.5%
	$3s3p^33d$	5.118(11)	2.1%	5.166(11)	2.1%
	total	2.374(13)	100%	2.504(13)	100%

from both KO and SO mechanisms. Note that channels from configurations of $3s^23p^3$, $3s3p^4$, $3p^5$, $3s^23p^23d$, $3s3p^33d$, $3s^23p^24s$, $3s^23p^24p$, $3s^23p^24d$, and $3p^43d$ contribute 97.9% and 99.2%, respectively, for levels of $2p_{3/2}^{-1}$ and $2p_{1/2}^{-1}$ by including contributions from KO and SO mechanisms, meaning that there are other weak channels for both hole levels, which are not given in Table IV.

Up to now, it is difficult to experimentally measure the level-to-level direct DAD rates for the inner-shell hole states. Available experiments in the literature [17,19,20] measured a fraction of the total DAD rates for the decay of Ar $2p^{-1}$ into triply charged ion. Viehhaus *et al.* [19] observed a branching ratio of 13(2)% for the decay into triply charged states by measuring the energy and angular distributions of the emitted electrons using electron coincidence spectroscopy. The number in parenthesis shows the errors in the last significant digit. This branching ratio was measured to be 15% by Nakano *et al.* [20], who used a multielectron coincidence technique with a magnetic bottle time-of-flight electron spectrometer. Brunken *et al.* [17] measured this value of 13% with uncertainty of $\sim 5\%$ by means of photoelectron-ion coincidence spectroscopy. Using our level-to-level rates, we obtained a direct DAD branching ratio of 11.4% by employing a KO mechanism and 12.0% including contributions from both KO and SO mechanisms for levels of $2p_{3/2}^{-1}$ and $2p_{1/2}^{-1}$. The branching ratio for cascade DAD is 2.9% for both levels. In total, this ratio is 14.3% for the KO mechanism and 14.9% including contributions from both mechanisms for both levels of Ar $2p^{-1}$. The average value for the configuration of Ar $2p^{-1}$ is the same as the results of the level-resolved double decay branching ratio. Both values of 14.3% and 14.9% are within the experimental errors [17,19,20]. Brunken *et al.* [17] also measured the level-resolved fraction of 12.5(4)% and 13.4(5)% for $2p_{3/2}^{-1}$ and $2p_{1/2}^{-1}$, respectively. Our level-resolved branching ratio is also within the experimental error bars [17]. The comparison is shown in Table V.

TABLE V. Branching ratios (BR) (%) for the direct and cascade double Auger decay of Ar $2p^{-1}$ and comparisons of the total theoretical double decay branching ratios with available experimental values in the literature. The numbers in parentheses for the experimental values give the errors in the last significant digit. Notations of *a* and *b* refer to results of only including KO and both KO and SO mechanisms, respectively.

Level	Direct BR	Cascade BR	Total double BR	Expt.
$2p_{3/2}^{-1}$	11.4% ^a , 12.0% ^b	2.9% ^a , 2.9% ^b	14.3% ^a , 14.9% ^b	12.5(4)% [17]
$2p_{1/2}^{-1}$	11.4% ^a , 12.0% ^b	2.9% ^a , 2.9% ^b	14.3% ^a , 14.9% ^b	13.4(5)% [17]
Average	11.4% ^a , 12.0% ^b	2.9% ^a , 2.9% ^b	14.3% ^a , 14.9% ^b	13(2)% [19], 15% [20], 13(5)% [17]

Lablanquie *et al.* [45] experimentally obtained a DAD probability of $9.1 \pm 1\%$ for $2p_{1/2}^{-1}$ and $9.4 \pm 1\%$ for $2p_{3/2}^{-1}$ hole level, which was underestimated compared with the experimental results [17,19,20]. The reason for the underestimation is that their experiment instrument is blind to Auger electrons with energies in the range 80–95 eV and therefore the contribution in this energy region is not included in their results. Earlier experiments [46,47] estimated this branching ratio to be $\sim 10\%$, which is lower than yet rather close to more recent accurate measurements [17,19,20]. We suggest that the accuracy of recent experiments [17,19,20] is higher than earlier ones [46,47].

This work represents a theoretical investigation of the direct DAD decay process of Ar inner-shell hole states by using a KO mechanism. Practical computations showed that KO is the dominant direct double decay mechanism and the theoretical results successfully explained the experimental measurements for the branching ratio of the double Auger decay into triply charged states of Ar³⁺. A previous theoretical prediction on the Auger decay of Ar $2p^{-1}$ which can be found in the literature was carried out by Kochur *et al.* [23], who employed a shake-off mechanism for the direct DAD process by using a straightforward Hartree-Fock model. They predicted a branching ratio of 0.8%, which strongly underestimated the decay fraction into the higher charged ion.

IV. CONCLUSION

In conclusion, large-scale CI calculations were carried out for the Auger decay including direct and cascade DAD processes of Ar $2p^{-1}$ hole states by using a distorted wave

method in the theoretical framework of perturbation. The complex transition amplitude for the direct double decay is decomposed into more practical formulas according to knock-out and shake-off mechanisms, which are generally considered to be the two main mechanisms in the direct DAD process. Practical computations indicated that the knock-out mechanism is dominant, which contributes to the probability an order of magnitude larger than that of shake-off. The main channels are due to levels belonging to the configurations of $3s^23p^3$ and $3s3p^4$, accounting for 66% and 18%, respectively, to the total probability. Direct and cascade DAD branching ratios of 12.0% and 2.9% are determined for the Auger decay of Ar $2p^{-1}$, resulting in a total double probability of 14.9% into triply charged states by including contributions from both the KO and SO mechanisms. Our theoretical results correctly explained the experimental results available in the literature. This work represents a theoretical implementation for the calculation of the direct DAD rates of Ar $2p^{-1}$ hole levels by using a KO mechanism. A previous theoretical work predicted a branching ratio of 0.8% by using an SO mechanism, which strongly underestimated the decay probability into the higher charged ion. More accurate and further experiments with higher accuracy are needed to obtain the configuration—or even level-resolved direct DAD rates—besides for the total double Auger decay probability.

ACKNOWLEDGMENTS

This work was supported by the National Natural Science Foundation of China under Grants No. 11274382, No. 11274383, and No. 11204376.

- [1] W. Ackermann *et al.*, *Nat. Photonics* **1**, 336 (2007).
- [2] T. Shintake *et al.*, *Nat. Photonics* **2**, 555 (2008).
- [3] P. Emma *et al.*, *Nat. Photonics* **4**, 641 (2010).
- [4] T. Ishikawa *et al.*, *Nat. Photonics* **6**, 540 (2012).
- [5] L. Young *et al.*, *Nature (London)* **466**, 56 (2010).
- [6] M. Hoener *et al.*, *Phys. Rev. Lett.* **104**, 253002 (2010).
- [7] G. Doumy *et al.*, *Phys. Rev. Lett.* **106**, 083002 (2011).
- [8] S. M. Vinko *et al.*, *Nature (London)* **482**, 59 (2012).
- [9] N. Rohringer *et al.*, *Nature (London)* **481**, 488 (2012).
- [10] B. Rudek *et al.*, *Nat. Photonics* **6**, 858 (2012).
- [11] H. Fukuzawa *et al.*, [arXiv:1210.0673](https://arxiv.org/abs/1210.0673) [Phys. Rev. Lett. (to be published)].
- [12] W. Xiang, C. Gao, Y. Fu, J. Zeng, and J. Yuan, *Phys. Rev. A* **86**, 061401(R) (2012).
- [13] T. A. Carlson and M. O. Krause, *Phys. Rev. Lett.* **14**, 390 (1965).
- [14] M. O. Krause, M. L. Vestal, W. H. Johnston, and T. A. Carlson, *Phys. Rev.* **133**, A385 (1964).
- [15] T. A. Carlson and M. O. Krause, *Phys. Rev. Lett.* **17**, 1079 (1966).
- [16] U. Alkemper, J. Doppelfeld, and F. von Busch, *Phys. Rev. A* **56**, 2741 (1997).
- [17] S. Brünken, Ch. Gerth, B. Kanngießner, T. Luhmann, M. Richter, and P. Zimmermann, *Phys. Rev. A* **65**, 042708 (2002).
- [18] S. Namba, N. Hasegawa, M. Nishikino, T. Kawachi, M. Kishimoto, K. Sukegawa, M. Tanaka, Y. Ochi, K. Takiyama, and K. Nagashima, *Phys. Rev. Lett.* **99**, 043004 (2007).
- [19] J. Viehhaus, S. Cvejanovic, B. Langer, T. Lischke, G. Prumper, D. Rolles, A. V. Golovin, A. N. Grum-Grzhimailo, N. M. Kabachnik, and U. Becker, *Phys. Rev. Lett.* **92**, 083001 (2004).

- [20] M. Nakano, Y. Hikosaka, P. Lablanquie, F. Penent, S. M. Huttula, I. H. Suzuki, K. Soejima, N. Kouchi, and K. Ito, *Phys. Rev. A* **85**, 043405 (2012).
- [21] R. Guillemin, S. Sheinerman, C. Bomme, L. Journel, T. Marin, T. Marchenko, R. K. Kushawaha, N. Trcera, M. N. Piancastelli, and M. Simon, *Phys. Rev. Lett.* **109**, 013001 (2012).
- [22] R. Guillemin, C. Bomme, T. Marin, L. Journel, T. Marchenko, R. K. Kushawaha, N. Trcera, M. N. Piancastelli, and M. Simon, *Phys. Rev. A* **84**, 063425 (2011).
- [23] A. G. Kochur, V. L. Sukhorukov, A. I. Dudenko, and Ph. V. Demekhin, *J. Phys. B* **28**, 387 (1995).
- [24] M. F. Gu, *Can. J. Phys.* **86**, 675 (2008).
- [25] M. S. Pindzola and D. C. Griffin, *Phys. Rev. A* **36**, 2628 (1987).
- [26] M. Ya. Amusia, I. S. Lee, and V. A. Kilin, *Phys. Rev. A* **45**, 4576 (1992).
- [27] T. Schneider, P. L. Chocian, and J. M. Rost, *Phys. Rev. Lett.* **89**, 073002 (2002).
- [28] J. Hozowska *et al.*, *Phys. Rev. Lett.* **102**, 073006 (2009).
- [29] W. Mehlhorn, in *Atomic Inner-Shell Physics*, edited by B. Crasemann (Plenum, New York, 1985), pp. 119–180.
- [30] J. Zeng, J. Yuan, and Q. Lu, *J. Phys. B* **34**, 2823 (2001).
- [31] J. Zeng and J. Yuan, *Phys. Rev. A* **66**, 022715 (2002).
- [32] J. Zeng, G. Dong, G. Zhao, and J. Yuan, *J. Phys. B* **37**, 2529 (2004).
- [33] W. Xiang, Y. Fu, C. Gao, and J. Zeng, *Phys. Scr.* **86**, 045302 (2012).
- [34] J. Bruneau, *J. Phys. B* **16**, 4135 (1983).
- [35] M. Ohno, *J. Electron Spectroscopy Related Phenomenon* **143**, 13 (2005).
- [36] A. H. Abdullah, A. M. El-Shemi, and A. Ghoneim, *Radiation Phys. Chem.* **68**, 697 (2003).
- [37] M. Jurvansuu, A. Kivimaki, and S. Aksela, *Phys. Rev. A* **64**, 012502 (2001).
- [38] T. X. Carroll, J. Hahne, T. D. Thomas, L. J. Sæthre, N. Berrah, J. Bozek, and E. Kukk, *Phys. Rev. A* **61**, 042503 (2000).
- [39] M. O. Krause and J. H. Oliver, *Phys. Chem. Ref. Data* **8**, 329 (1979).
- [40] J. Nordgren, H. Ågren, C. Nordling, and K. Siegbaha, *Phys. Scr.* **19**, 5 (1979).
- [41] Gy. Viktor, L. Toth, S. Ricz, A. Kover, J. Vegh, and B. Sulik, *J. Electron Spectroscopy Related Phenomenon* **83**, 235 (1997).
- [42] H. M. Koppe, A. L. D. Kilcoyne, J. Feldhaus, and A. M. Bradshaw, *J. Electron Spectroscopy Related Phenomenon* **75**, 97 (1995).
- [43] J. Zeng, J. Yuan, and Q. Lu, *Phys. Rev. E* **64**, 066412 (2001).
- [44] S. Sheinerman *et al.*, *J. Phys. B* **43**, 115001 (2010).
- [45] P. Lablanquie *et al.*, *J. Electron Spectroscopy Related Phenomenon* **156**, 51 (2007).
- [46] T. Hayaishi, E. Murakami, Y. Morioka, E. Shigemasa, A. Yagishita, and F. Koike, *J. Phys. B* **28**, 1411 (1995).
- [47] M. J. Van der Wiel and G. Wiebes, *Physica* **53**, 225 (1971).